to explore these findings in skin samples harbouring the AQP5^{Ile45Ser} variant. Interestingly, molecular dynamic simulations have reported a role of HA in the regulation of water permeability of AQP3, another member of the Aquaporin protein family expressed in skin (Zhang et al, 2021).

Altogether, this data proposes a role for AQP5 in the regulation of actin cytoskeleton dynamics in the skin, while deepening our understanding of the unique molecular characteristics of the palmoplantar epidermis and how it contrasts to body skin.

DATA AVAILABILITY STATEMENT

No large datasets were generated or analyzed during this study.

KEYWORDS

BioID; CD44; Hyaluronic acid; pMLC2; Stress fibres

ORCIDs

Laura Ramos: http://orcid.org/0009-0009-4821-081X
Andrew P South: http://orcid.org/0000-0001-7650-0835
Edel O'Toole: http://orcid.org/0000-0002-4084-4836
David Kelsell: http://orcid.org/0000-0002-9910-7144
Diana Blaydon: http://orcid.org/0000-0002-9998-2563

CONFLICT OF INTEREST

EOT is a consultant for Kamari Pharma, Palvella Therapeutics, and Unilever (unrelated to this work) and receives grants to her institution from Kamari Pharma, Palvella Therapeutics, and Azitra. All other authors state no conflict of interest.

ACKNOWLEDGMENTS

This work is supported by a grant awarded to DCB from the British Skin Foundation (011/S/18) as well as by a grant awarded to DPK from the Medical Research Council (MR/S009914/1). The authors would like to thank Anita Lundström (Dermatology and Venereology, Department of Public Health and Clinical Medicine, Umeå University, Umeå, Sweden) for providing the AQP5^{Ala38Glu} palm biopsy. The authors would also like to thank Roberto Buccafusca from the School of Biological and Behavioural Chemical Sciences Mass Spectrometry Laboratory and the Blizard Advanced Light Microscopy core facilities for their collaboration in this project.

AUTHOR CONTRIBUTIONS

Conceptualization: DCB, DPK; Funding Acquisition: DCB, DPK; Investigation: LRdC, DCB; Resources: APS, EAO; Supervision: DCB, DPK; Writing - Original Draft Preparation: LRdC; Writing - Review and Editing: APS, EAO, DPK, DCB

***Laura Ramos del Caño*[1], *Andrew P. South*[2], *Edel A. O'Toole*[1], *David P. Kelsell*[1] *and Diana C. Blaydon*[1,*]**

[1]*Centre for Cell Biology and Cutaneous Research, Blizard Institute, The Faculty of Medicine and Dentistry, Queen Mary University of London, London, United Kingdom; and* [2]*Department of Dermatology & Cutaneous Biology, Thomas Jefferson University, 233 South Tenth Street BLSB 406, Philadelphia, Pennsylvania, USA*
[*]*Corresponding author e-mail: d.blaydon@qmul.ac.uk*

SUPPLEMENTARY MATERIAL

Supplementary material is linked to the online version of the paper at www.jidonline.org, and at https://doi.org/10.1016/j.jid.2024.02.028.

REFERENCES

Blaydon DC, Lind LK, Plagnol V, Linton KJ, Smith FJ, Wilson NJ, et al. Mutations in AQP5, encoding a water-channel protein, cause autosomal-dominant diffuse nonepidermolytic palmoplantar keratoderma. Am J Hum Genet 2013;93:330–5.

Bourguignon LY. Hyaluronan-mediated CD44 activation of RhoGTPase signaling and cytoskeleton function promotes tumor progression. Semin Cancer Biol 2008;18:251–9.

Jensen HH, Holst MR, Login FH, Morgen JJ, Nejsum LN. Ectopic expression of aquaporin-5 in noncancerous epithelial MDCK cells changes cellular morphology and actin fiber formation without inducing epithelial-to-mesenchymal transition. Am J Physiol Cell Physiol 2018;314:C654–61.

Ning W, Muroyama A, Li H, Lechler T. Differentiated daughter cells regulate stem cell proliferation and fate through intra-tissue tension. Cell Stem Cell 2021;28:436–452.e5.

Roux KJ, Kim DI, Raida M, Burke B. A promiscuous biotin ligase fusion protein identifies proximal and interacting proteins in mammalian cells. J Cell Biol 2012;196:801–10.

Shatirishvili M, Burk AS, Franz CM, Pace G, Kastilan T, Breuhahn K, et al. Epidermal-specific deletion of CD44 reveals a function in keratinocytes in response to mechanical stress. Cell Death Dis 2016;7:e2461.

Totsukawa G, Yamakita Y, Yamashiro S, Hartshorne DJ, Sasaki Y, Matsumura F. Distinct roles of ROCK (rho-kinase) and MLCK in spatial regulation of MLC phosphorylation for assembly of stress fibers and focal adhesions in 3T3 fibroblasts. J Cell Biol 2000;150:797–806.

Yasaka N, Furue M, Tamaki K. CD44 expression in normal human skin and skin tumors. J Dermatol 1995;22:88–94.

Yonemura S, Hirao M, Doi Y, Takahashi N, Kondo T, Tsukita S, et al. Ezrin/radixin/moesin (ERM) proteins bind to a positively charged amino acid cluster in the juxta-membrane cytoplasmic domain of CD44, CD43, and ICAM-2. J Cell Biol 1998;140:885–95.

Zhang H, Cai W, Shao X. Regulation of aquaporin-3 water permeability by hyaluronan. Phys Chem Phys 2021;23:25706–11.

See related commentary on pg 1912

Genetic Variants Associated with Sweat Gland Phenotypes in 6210 Han Chinese Individuals

Journal of Investigative Dermatology (2024) **144,** 2096–2100; doi: 10.1016/j.jid.2024.02.037

Abbreviations: CI, confidence interval; SGD, sweat gland density

Accepted manuscript published online 10 April 2024; corrected proof published online 18 May 2024

TO THE EDITOR

Sweat glands are widely distributed across human skin, playing an essential role in thermoregulation and body temperature maintenance, whereas sweat gland dysfunction is associated with

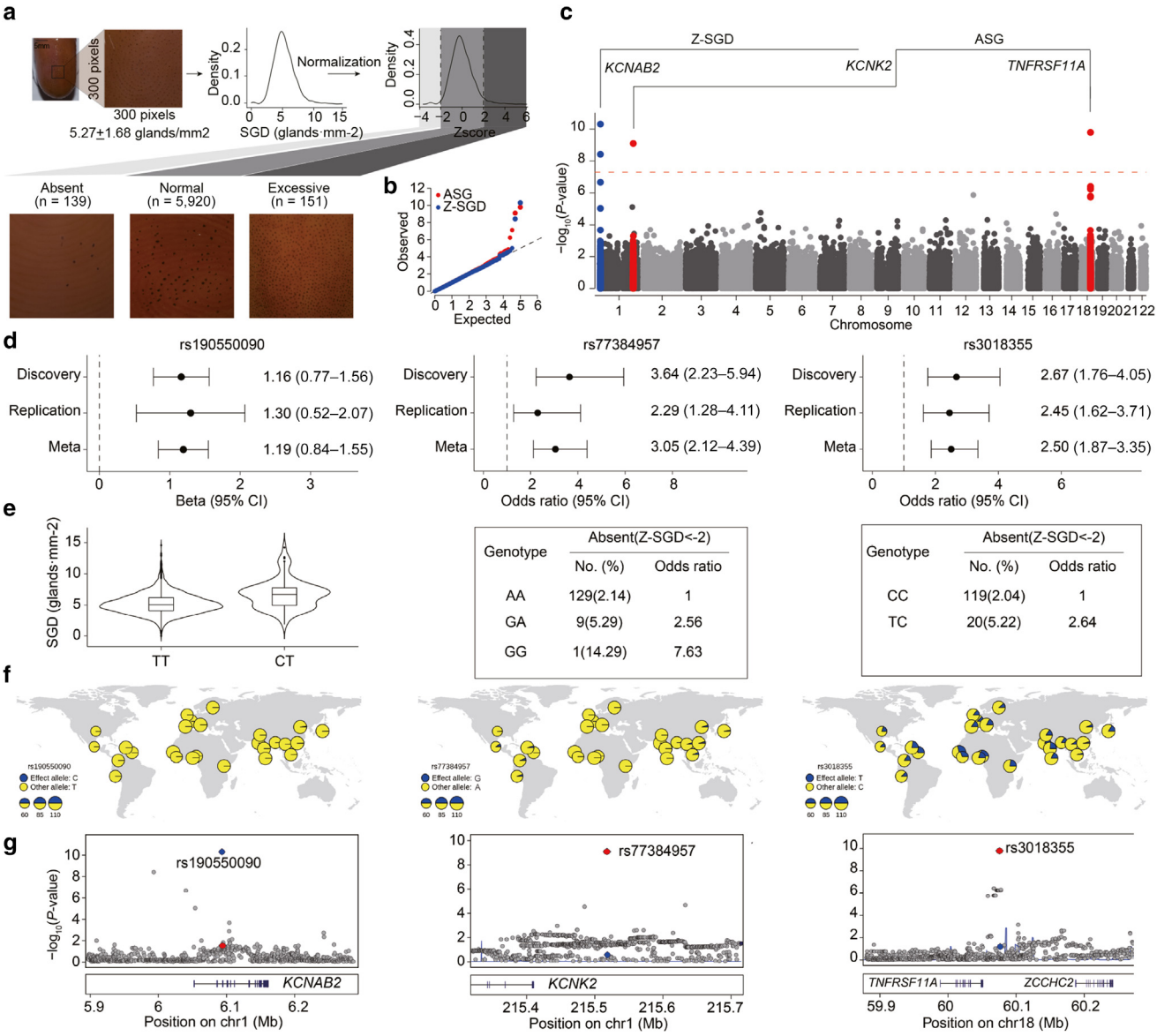

Figure 1. Phenotypic and genetic effects of sweat gland phenotypes. (**a**) The definition and distribution of the sweat gland phenotypes. Bar = 5 mm. (**b**) The Q−Q plot of the sweat gland phenotypes. ASG represents the absence of active sweat gland phenotype, whereas Z-SGD represents the Z-transformed SGD phenotype. (**c**) The Manhattan plots in the meta-analysis of the sweat gland phenotypes. The horizontal red line represents the genome-wide significant threshold ($P < 5\times10^{-8}$). The genomic loci associated with the absence of active sweat gland phenotype and Z-SGD phenotypes are displayed in red and blue, respectively. (**d**) The forest plot displaying the ORs and confidence intervals of the sweat gland phenotype signals in both the discovery and replication cohorts. (**e**) The alleles of sweat gland phenotype signals and their corresponding phenotype directions. For rs190550090, the allele distribution is shown on the left, indicating the SGD of individuals with different alleles. OR of SNP rs77384957 on the absence of active sweat gland phenotype is depicted in the middle. Similarly, the OR of rs3018355 on the absence of active sweat gland phenotype is presented on the right. (**f**) The allele frequency map for rs190550090, rs77384957, and rs3018355. (**g**) The LocusZoom plots of the 3 identified marker SNPs (rs190550090 at 1p36.3, rs77384957 at 1q41, and rs3018355 at 18q21.3). Results ($-\log_{10}P$) are shown for SNPs in the region flanking 200 kb on either side of the marker SNPs. The markers' significance in the Z-SGD phenotype is represented by the blue color, which indicated the −log10 *P*-value. Conversely, the red color represents the −log10 *P*-value of the markers in the absence of active sweat gland phenotype. ASG, absence of sweat gland; Z-SGD, Z-transformed sweat gland density.

various skin disorders, such as hyperhidrosis and anhidrosis (Asahina et al, 2015). Sweat gland density (SGD) varies significantly between and within ethnic groups (Lee et al, 2010). Despite the estimated heritability of SGD up to 0.66 (Scobbie and Sofaer, 1987), the underlying genetic factors and mechanisms responsible for this variation remain largely unexplored. In this study, we report the GWAS on SGD, involving 6210 Han Chinese individuals from 2 independent cohorts: the Taizhou Longitudinal Study (n = 3883) and the National Survey of Physical Traits (n = 2327) (Supplementary Figure S1). Genetic principal component analysis did not detect population substratification (Supplementary Figure S2). Ethical approval was obtained from the Ethics Committees of Fudan University (14117) and the Shanghai Institutes for Biological Sciences (ER-SIBS-261410), and all participants provided written informed consent.

The classical starch iodine solution (Muller and Kierland, 1959) method

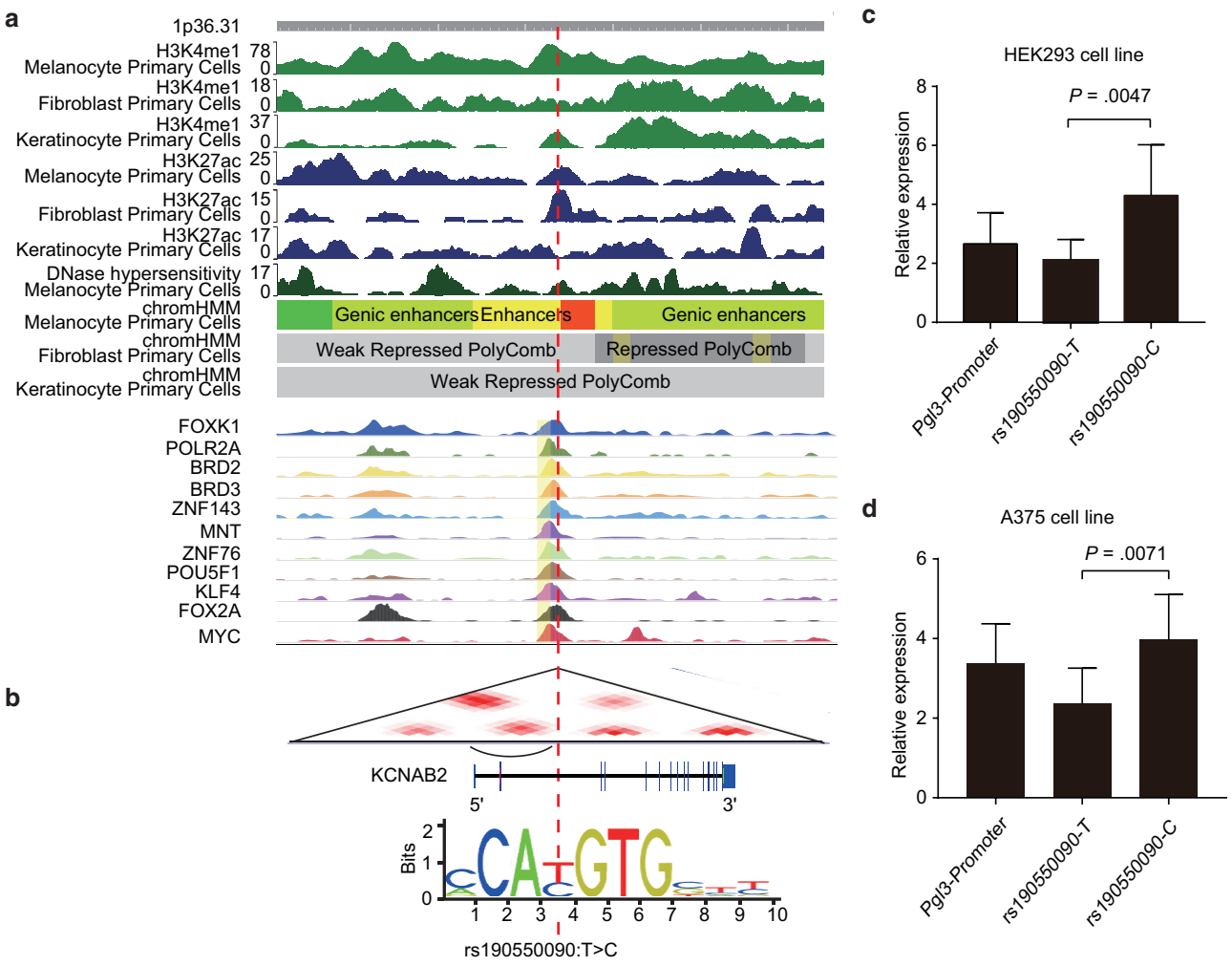

Figure 2. Functional annotation and experimental validation of the SG phenotype signals. (**a**) Functional annotation of Z-SGD signal rs190550090. Multiple histone modifications bind to rs190550090 (top panel). ChIP-Seq results show that rs190550090 is the transcription factor–binding site of ZNF76, POU5F1, MYC, KLF4, and FOXA2, etc (bottom panel). (**b**) Z-SGD signal rs190550090 has an interaction with the promoter of *KCNAB2* in ovary cell line presented by 3DIV (Yang et al, 2018), and it falls in the canonical E-box (CATGTG/CACGTG) motif, which is a regulatory element that is recognized and bound by transcription factors to activate gene transcription (Massari and Murre, 2000). (**c**) Luciferase reporter assays confirmed that the transcriptional activity of the enhancer containing the rs190550090-derived allele C was significantly higher than that of the corresponding ancestral allele T in the HEK293 and A375 cell lines (**d**). ChIP-Seq, chromatin immunoprecipitation sequencing; HEK, human embryonic kidney; SG, sweat gland; Z-SGD, Z-transformed sweat gland density.

was applied to detect active sweat glands. An advanced image analysis was then performed to quantify the number of glands per mm^2 (Figure 1a and Supplementary Materials and Methods). SGD demonstrated a moderately right-skewed distribution in both cohorts (mean = 5.02 ± 1.47 to 5.37 ± 1.70 glands/mm^2) (Supplementary Table S1). Notably, females displayed a trend toward higher *Z*-transformed SGD, representing an increase of 0.4 SDs ($P < .006$) (Supplementary Table S2). *Z*-transformed SGD decreased by 0.3–0.4 SDs for every 10-year increase in age ($P < 2.4 \times 10^{-12}$). SNP-based heritability was estimated at 0.35, confirming the genetic component detectable by our microarray data.

Our GWAS did not show sign of genomic inflation (lambda < 1.01) (Figure 1b) and revealed 1p36.3 to be significantly associated with *Z*-transformed SGD in Taizhou Longitudinal Study (lead SNP rs190550090, $P = 1.01 \times 10^{-8}$), which was successfully replicated in National Survey of Physical Traits with similar allelic effects ($P = 1.03 \times 10^{-3}$) (Figure 1c and d). In the meta-analysis of 2 cohorts, the association at 1p36.3 was further strengthened ($\beta = 1.19$, $P = 4.98 \times 10^{-11}$) (Figure 1c).

SGD of rs190550090-CT carriers was 1.52 glands/mm^2 higher than that of rs190550090-TT carriers (Figure 1e). The frequency of derived C allele was low (~1% in our sample), consistent with that of East Asians in the 1000 Genomes Project. The C allele was virtually undetected in non–East Asian cohorts, suggesting population specificity (Figure 1f and Supplementary Table S3). Rs190550090 is located in the intron of *KCNAB2*, a gene involved in acetylcholine release, which is responsible for triggering sweat gland secretion (Shibasaki and Crandall, 2001).

Interestingly, 139 participants had absence of sweat glands (< −2 SD), with a significantly higher risk of dry skin based on questionnaires (OR = 1.03, 95% confidence interval

[CI] = 1.01−1.05, $P = .003$) and susceptibility to crack or wrinkle skin (OR = 1.02, 95% CI = 1.00−1.03, $P = .004$). In addition, they displayed a higher number of facial pigment spots ($\beta = 0.03$, 95% CI = 0.01−0.05, $P = .003$). Further meta-analysis of absence of sweat gland identified 2 significantly related loci. The first locus is at 1q41 downstream of *KCNK2*, another member of the potassium channel family playing a crucial role in heat-sensitive sweating (Kang et al, 2005). The derived G allele of rs77384957 was associated with an increased risk of the absence of sweat gland (OR = 3.05, 95% CI = 2.12−4.39, $P = 1.98 \times 10^{-9}$), with consistent effects in both cohorts ($P_{\text{National Survey of Physical Traits}} = 2.32 \times 10^{-7}$; $P_{\text{Taizhou Longitudinal Study}} = 5.28 \times 10^{-3}$) (Figure 1d and e). The frequency of G allele was low in our sample and in the 1000 Genomes Project East Asians, whereas it was nearly absent outside of East Asia (Figure 1f and Supplementary Table S3). The second locus is at 18q21.3 downstream of *TNFRSF11A*, inducing the activation of NF-kB, known to regulate sweat gland development and sweat production (Lu et al, 2016). The T allele of rs3018355 was associated with an increased risk of the absence of sweat gland (OR = 2.50, 95% CI = 1.87−3.35, $P = 8.25 \times 10^{-10}$). The homozygote TT was not observed owing to the low allelic frequency (1%), whereas it was common in populations outside of East Asia ($f_{\text{European}} = 0.14$; $f_{\text{African}} = 0.25$) (Figure 1f and Supplementary Table S3). No genome-wide significant loci associated with excessive sweat gland (n = 151; >2 SD) were found. For the 3 nominated SNPs mentioned earlier, a sex-stratified analysis revealed consistent SNP effects across both sexes.

Fine-mapping analysis showed that all of the 3 SNPs had high posterior probabilities (>0.95) with regulatory roles in gene expression (Supplementary Table S3). Specifically, rs190550090 region showed distinct active enhancer signatures, and chromatin immunoprecipitation−sequencing data (Landt et al, 2012) further revealed its role as a binding site for several transcription factors, including ZNF76, POU5F1, MYC, KLF4, and FOXA2 (Figure 2a). Hi-C study demonstrated that rs190550090 interacts with the promoter of *KCNAB2*, and it is located in the canonical E-box motif that is known to be recognized and bound by transcription factors, thereby activating gene transcription (Massari and Murre, 2000) (Figure 2b). We performed luciferase reporter assay in human embryonic kidney 293 and A375 cell lines, and the results showed that the transcriptional activity of the sequence containing C allele exhibited significantly higher than that containing T allele in both cell lines, which verified the potential modulating activity of rs190550090 (Figure 2c and d). Detailed results for rs77384957 and rs3018355 are provided in Supplementary Text and Supplementary Figure S3. No significant positive selection signals were detected at these 3 loci, as expected owing to the low allelic frequencies (Supplementary Figure S4 and Supplementary Table S4).

In summary, we identified 3 loci associated with sweat gland phenotypes. Two are specific to East Asians and situated near potassium channel genes, highlighting the channels' functional role in sweat gland development and the risk of chronic idiopathic anhidrosis. These loci may exhibit different single nucleotide variations in non−East Asian populations, warranting further investigation through population-specific candidate gene analysis. The third locus, prevalent in non−East Asian populations and showing uniform linkage disequilibrium patterns, suggests a more detectable association in these groups. Despite the low allele frequencies of these loci, which may inherently be more susceptible to chance associations than common alleles, our findings enhance the understanding of genetic influences on sweat gland diversity and their potential impact on skin-related conditions.

DATA AVAILABILITY STATEMENT

The GWAS summary statistics can be accessed from the National Omics Data Encyclopedia (http://www.biosino.org/node/) using the project identification document OEP004627. Please note that the usage of data must fully comply with the Regulations on Management of Human Genetic Resources in China. Owing to privacy concerns and restrictions imposed by the institutional review board, individual genotype and phenotype data cannot be shared. However, other relevant data supporting the key findings of this study can be found in the letter and supplementary materials or obtained from the corresponding author upon reasonable request.

KEYWORDS

GWAS; SNP; Sweat gland

ORCIDs

Wenyan Chen: http://orcid.org/0000-0002-4821-9306
Jinxi Li: http://orcid.org/0000-0002-1366-9593
Ke Xu: http://orcid.org/0000-0002-0408-1659
Junyu Luo: http://orcid.org/0000-0003-2206-1931
Mengran Wang: http://orcid.org/0000-0002-9281-9501
Yu Liu: http://orcid.org/0000-0001-7110-127X
Fudi Wang: http://orcid.org/0000-0002-0208-3343
Siyuan Du: http://orcid.org/0000-0003-1602-1669
Wenjie Xu: http://orcid.org/0009-0005-4244-2733
Jieyu Ge: https://orcid.org/0000-0002-1070-2087
Yi Li: https://orcid.org/0000-0002-2448-9176
Bingfei Fu: https://orcid.org/0009-0006-4155-9478
Xiangyang Xue: http://orcid.org/0000-0002-4897-9209
Jingze Tan: http://orcid.org/0009-0000-4447-8653
Yajun Yang: http://orcid.org/0000-0001-5713-0103
Jiucun Wang: http://orcid.org/0000-0003-2765-0620
Li Jin: http://orcid.org/0000-0001-9201-2321
Zhaohui Yang: http://orcid.org/0000-0003-0958-4439
Fan Liu: http://orcid.org/0000-0001-9241-8161
Sijia Wang: http://orcid.org/0000-0001-6961-7867

CONFLICT OF INTEREST

The authors state no conflict of interest.

ACKNOWLEDGMENTS

We thank members of the Wang laboratory for helpful discussions. This work was supported by the Strategic Priority Research Program of the Chinese Academy of Sciences (grant number XDB38020400 to SW), CAS Project for Young Scientists in Basic Research (grant number YSBR-077 to SW), National Science and Technology Basic Research Project (grant number 2015FY111700 to SW), CAMS Innovation Fund for Medical Sciences (2019-I2M-5-066 to SW), National Natural Science Foundation of China (32070579 and 32370664 to ZY), Natural Science Foundation of Henan (222300420067 to ZY), and National Natural Science Foundation of China (32200482 to JLi). Correspondence regarding the luciferase assays and population comparative analyses should be addressed to ZY (yangzh@zzu.edu.cn) and FL (fliu@nuass.edu.sa), respectively.

AUTHOR CONTRIBUTIONS

Conceptualization: SW; Data Curation: WC; Methodology: WC, SW, FL; Data collection: WC, KX, JLu, MW, YuL, FW, LW, SD, WX, JG; Formal analysis: WC; Visualization: SW, WC, JLi; Funding Acquisition: SW; Supervision: SW, FL, ZY; Writing - Original Draft Preparation: WC, SW, FL; Writing - Review and Editing: WC, JLi, KX, JLu, MW, YuL, FW, SD, WX, JG, YiL, BF, XX, JT, YY, JW, LJ, ZY, FL, SW

Wenyan Chen[1,10], Jinxi Li[2,10], Ke Xu[3,10], Junyu Luo[1], Mengran Wang[1], Yu Liu[1], Fudi Wang[1], Siyuan Du[1], Wenjie Xu[1], Jieyu Ge[1], Yi Li[1], Bingfei Fu[4], Jingze Tan[5], Yajun Yang[5], Jiucun Wang[2,6,7], Xiangyang Xue[4], Li Jin[2,6,7], Zhaohui Yang[3], Fan Liu[8] and Sijia Wang[1,9,*]

[1]CAS Key Laboratory of Computational Biology, Shanghai Institute of Nutrition and Health, University of Chinese Academy of Sciences, Chinese Academy of Sciences, Shanghai, China; [2]State Key Laboratory of Genetic Engineering, Human Phenome Institute, Zhangjiang Fudan International Innovation Center, Fudan University, Shanghai, China; [3]Academy of Medical Science, Zhengzhou University, Zhengzhou, China; [4]Institute of Intelligent Media Computing, School of Computer Science, Fudan University, Shanghai, China; [5]Ministry of Education Key Laboratory of Contemporary Anthropology, Department of Anthropology and Human Genetics, School of Life Science, Fudan University, Shanghai, China; [6]Fudan University Taizhou Institute of Health Sciences, Taizhou, China; [7]Research Unit of Dissecting the Population Genetics and Developing New Technologies for Treatment and Prevention of Skin Phenotypes and Dermatological Diseases (2019RU058), Chinese Academy of Medical Sciences, Shanghai, China; [8]Department of Forensic Sciences, College of Criminal Justice, Naif Arab University for Security Sciences, Riyadh, Saudi Arabia; and [9]Center for Excellence in Animal Evolution and Genetics, Chinese Academy of Sciences, Kunming, China

[10]These authors contributed equally to this work.

*Corresponding author. e-mail: wangsijia@picb.ac.cn

SUPPLEMENTARY MATERIAL

Supplementary material is linked to the online version of the paper at www.jidonline.org, and at https://doi.org/10.1016/j.jid.2024.02.037.

REFERENCES

Asahina M, Poudel A, Hirano S. Sweating on the palm and sole: physiological and clinical relevance. Clin Auton Res 2015;25:153–9.

Kang D, Choe C, Kim D. Thermosensitivity of the two-pore domain K+ channels TREK-2 and TRAAK. J Physiol 2005;564:103–16.

Landt SG, Marinov GK, Kundaje A, Kheradpour P, Pauli F, Batzoglou S, et al. ChIP-seq guidelines and practices of the ENCODE and modENCODE consortia. Genome Res 2012;22:1813–31.

Lee JB, Kim TW, Shin YO, Min YK, Yang HM. Effect of the heat-exposure on peripheral sudomotor activity including the density of active sweat glands and single sweat gland output. Korean J Physiol Pharmacol 2010;14:273–8.

Lu CP, Polak L, Keyes BE, Fuchs E. Spatiotemporal antagonism in mesenchymal-epithelial signaling in sweat versus hair fate decision. Science 2016;354:aah6102.

Massari ME, Murre C. Helix-loop-helix proteins: regulators of transcription in eucaryotic organisms. Mol Cell Biol 2000;20:429–40.

Muller SA, Kierland RR. The use of a modified starch-iodine test for investigating local sweating responses to intradermal injection of methacholine. J Invest Dermatol 1959;32:126–8.

Scobbie RB, Sofaer JA. Sweat pore count, hair density and tooth size: heritability and genetic correlation. Hum Hered 1987;37:349–53.

Shibasaki M, Crandall CG. Effect of local acetylcholinesterase inhibition on sweat rate in humans. J Appl Physiol (1985) 2001;90:757–62.

Yang D, Jang I, Choi J, Kim MS, Lee AJ, Kim H, et al. 3DIV: a 3D-genome Interaction Viewer and database. Nucleic Acids Res 2018;46:D52–7.

Trends in Age at Melanoma Diagnosis according to Thickness and Histologic Subtype Have Implications for Causality and Control

JID Open

Journal of Investigative Dermatology (2024) **144,** 2100–2103; doi: 10.1016/j.jid.2024.02.003

TO THE EDITOR

All approaches to cancer screening incorporate some consideration of age because aging is arguably the single most important nonmodifiable risk factor for many cancers, including melanoma. Information on the distribution of age at diagnosis is therefore important for designing risk-stratified approaches to early detection. However, a key issue is whether there exist differences in the lethality of melanomas arising at different ages. Recently, concerns have been raised that early detection activities for melanoma contribute to overdiagnosis, whereby indolent tumors that pose little or no risk to the patient are diagnosed and treated, yet tumors with poor prognosis are missed (Olsen et al, 2022; Welch et al, 2021; Whiteman et al, 2022). The strongest predictors of poor prognosis are thickness and nodular subtype. We therefore sought to examine trends in the age at diagnosis of invasive melanoma by thickness and histologic subtype in 2 populations exposed to different levels of ambient UVR (the United States [US] White population and the Queensland, Australia population), with the aim of informing age-based risk stratification programs intended to detect lethal melanomas early in their course.

We obtained case listings of all melanoma diagnoses over the period 1999–2018 for the US White population from the Surveillance, Epidemiology, and End Results program of the National Cancer Institute (9 registries, covering approximately 9.4% of the

Abbreviations: LMM, lentigo malignant melanoma; NM, nodular melanoma; SSM, superficial spreading melanoma; US, United States

Accepted manuscript published online 22 February 2024; corrected proof published online 14 March 2024

SUPPLEMENTARY TEXT

Our fine-mapping analysis using PAINTOR confirmed that our identified SNPs all had high posterior probabilities of causality ($P > .95$) (Supplementary Table S3). Functional annotations further substantiated their regulatory role (Supplementary Table S3). The absence of active sweat glands phenotype associated SNP rs77384957 was found within histone modifications associated with active regulatory elements, such as H3K4me3, H3K4me1, and H3K27ac (Supplementary Figure S3a). In addition, analysis of publicly available chromatin immunoprecipitation-sequencing data (Landt et al, 2012) provided further support for rs77384957, revealing its role as a binding site for several transcription factors, including BRD4, MED1, RELA, PPARG, CTCF, AHR, and SMARCA4 (Supplementary Figure S3b). For another absence of active sweat glands phenotype—associated SNP rs3018355, we observed that it is the transcription-binding site of ZNF384 (Supplementary Figure S3c). These compelling lines of evidence strongly support that rs77384957 affects the absence of active sweat glands by regulating the expression of target gene.

We also conducted linkage disequilibrium (LD) analysis for both LD r^2 and D′ in East Asian, European, and African samples from the 1000 Genomes Project (Supplementary Figure S5). LD heatmap confirms low LD between our identified SNPs and other SNPs in these genomic regions and showed similar LD patterns between supper populations. The first 2 loci are both located near potassium channel genes, suggesting the functional role of potassium in sweat gland development, although different variants at the same genomic regions may exist in non—East Asian populations owing to allelic heterogeneity. For the third locus, we expect that the association with sweat gland phenotypes may be more readily detectable in other populations.

To further explore the SNPs we identified and those in high LD with them ($r^2 > 0.4$), we conducted a comprehensive cross-referencing with available GWAS summary statistics. This included data from the GWAS Catalog, over 700 GWASs from the UK Biobank , and 280 GWASs from the Biobank Japan. Our cross-reference analysis indicated that none of our 3 identified SNPs reached genome-wide significance. However, an interesting observation was made in the GWAS Catalog. One of our identified that absence of sweat gland hits, located at 18q21.3 (rs3018355) and more frequent outside of Asia, exhibited a nominally significant association with excessive hair growth ($P = .01$) (Endo et al, 2018). This suggests a potential shared genetic basis between this absence of sweat gland and excessive hair growth.

SUPPLEMENTARY MATERIALS AND METHODS

Study subjects

This study involved 6210 Han Chinese individuals from 2 separate cohorts: the Taizhou Longitudinal Study (n = 3883) and the National Survey of Physical Traits (n = 2327). The Taizhou Longitudinal Study cohort was used for discovery purposes, whereas the National Survey of Physical Traits cohort served as a validation cohort. The individuals in the discovery cohort had an average age of 54.80 ± 10.23 years, with 64.23% being females. In the replication cohort, participants had an average age of 50.13 ± 13.44 years, and 62.53% were females.

Genotyping, quality control, and imputation

We employed the GENEray DNA extraction kit to extract DNA from blood samples obtained from participants. The first-stage samples from the Taizhou cohort (TZ1) were genotyped using the Illumina Human Omni Zhonghua8V1.1 chip, which covers 887,270 SNPs. For the second and third stages of the Taizhou cohorts (TZ2 and TZ3) as well as the Henan and Guangxi cohorts, we used the Illumina Global Screening Array with 707,146 SNPs for genotyping. The imputation was performed using IMPUTE2 (Howie et al, 2009), with individuals from the 1000 Genomes phase 3 dataset serving as a reference set. After imputation, we excluded variants with an INFO score below 0.8 or a certainty score below 0.9 to ensure data quality. Our quality control procedures were carried out using PLINK, version 1.9 (Chang et al, 2015). During this phase, we removed SNPs that had a genotype missing rate >0.02, had a minor allele frequency <0.01, or failed the Hardy—Weinberg equilibrium test ($P < 1\times10^{-5}$). Furthermore, we did not detect any samples exhibiting >5% missing data, signs of cryptic relatedness, or discrepancies in reported sex. After applying these stringent filtering criteria, the Taizhou Longitudinal Study cohort (3883 individuals) encompassed 7,057,720 variants. Similarly, the National Survey of Physical Traits cohort (2327 individuals) retained a total of 8,039,700 variants.

Phenotyping: sweat gland phenotype

Written consent was requested before the participation in the study.

Phenotyping: sweat gland density

Among humans, there are significant differences in the distribution of eccrine glands across various body parts, with the highest concentration observed in the palms and soles (Sato and Dobson, 1970). Sweating on the palms and soles is believed to be a useful indicator of sympathetic function and limbic activity in autonomic and psychiatric disorders (Asahina et al, 2015). In this study, we recorded sweat gland phenotype on the fingertips using the starch-iodine reaction owing to its practicality and simplicity. This allowed us to assess the palmar sympathetic sweat responses or activity for each participant. Furthermore, 2-dimensional photographs were captured using a Nikon D400 digital camera. To quantify individual sweat gland density (SGD), which represents interindividual variations, we developed a robust automated image analysis method.

In our study, we utilized a commonly used noninvasive method on the basis of starch/iodine reactions to measure sweat glands (Juniperet al, 1964). First, we collected the index fingers of participants' left hand and cleaned them using 70% ethanol. After cleaning, we applied an iodine/ethanol solution carefully to the fingertips and allowed it to air dry for approximately 1 minute. Next, we applied a thin film composed of a 1:1 mixture of starch and castor oil to the fingertips. As sweat was secreted from the sweat glands, it broke the oil barrier, causing the starch—iodine reaction. This reaction resulted in the

formation of distinct black dots, indicating the activated sweat glands. Approximately 2.5 minutes later, we captured high-resolution pictures of the fingers using a Nikon D400 digital camera. To ensure accurate sample tracking and picture alignment, each finger was labeled with a subject-specific code, which was included in the picture. This labeling facilitated easy tracking and adjustment of picture size on the basis of the reference label. For further analysis, only high-quality images (left panel in Supplementary Figure S6) were considered. The center of the fingerprint pattern typically exhibited superior resolution, so we cropped a square target area around this region (Figure 1a). We developed an automated image analysis pipeline using MATLAB to count the number of sweat glands in each cropped image. This pipeline involved converting the original images to grayscale, balancing the grayscale images, and labeling and counting the sweat glands. By implementing this MATLAB pipeline, we efficiently analyzed the distribution of sweat glands within the cropped images. To validate the accuracy of our image recognition method, we compared the sweat glands identified through image recognition with those manually labeled. The results demonstrated a strong correlation and consistent agreement between the number of sweat glands recognized by our image recognition method and the manually labeled ones (Supplementary Figure S7), confirming the reliability and effectiveness of our approach.

Phenotyping: the absence of active sweat glands

To determine the absence of active sweat glands, we utilized *Z* scores to normalize the SGD. The Z score is calculated by subtracting the overall average SGD for all individuals and dividing the result by the SD of all measured SGDs. The formula for calculating the Z score is as follows: Z score = $(SGD_i - \text{mean})/SD$.

In our study, the absence of active sweat glands represented a binary phenotype, categorized as either the absence of active sweat glands or normal active sweat glands (Figure 1a). The case sample, indicating the absence of active sweat gland, was defined as SGD $\leq$ 1.88 glands/mm^2 and corresponding Z score ≤ -2. On the other hand, the control sample, representing normal active sweat gland, was defined as SGD $>$ 1.88 glands/mm^2 and corresponding Z score > -2.

Phenotyping: excessive active sweat gland

The definition of excessive active sweat gland follows a similar approach. Excessive active sweat gland is also categorized as a binary phenotype: excessive active sweat glands and normal active sweat glands (Figure 1a). The case sample represents the excessive active sweat gland and is defined as SGD $\geq$ 8.75 glands/mm^2, along with the corresponding Z score > -2. On the other hand, the control sample represents normal active sweat gland and is defined as SGD $<$ 8.75 glands/mm2, along with the corresponding Z score < 2.

Statistical analyses

Statistical analyses: population stratification analysis. Genomic principal component analysis was performed to adjust for population stratification with EIGENSTRAT (Price et al, 2006). To reduce the computer calculations and reduce potential bias introduced by LD structure, SNPs were first pruned for LD (pairwise $r^2 < 0.2$) by PLINK (Chang et al, 2015). The Tracy–Widom statistics from EIGENSTRAT identified 4 statistically significant eigenvectors ($P < .05$) (Supplementary Figure S8).

Statistical analyses: association analyses. The Tracy–Widom statistics from EIGENSTRAT identified 4 statistically significant eigenvectors ($P < .05$) (Supplementary Figure S8). We therefore included these 4 main principal components as covariates in our GWAS in addition to sex and age. GWAS was performed using linear regression for the quantitative trait Z-transformed sweat gland density and logistic regression for binary traits (active sweat glands and excessive sweat gland) assuming additive allelic effects using PLINK, version 1.9. The GWAS summary statistics from the discovery cohort and the replication cohort were meta-analyzed focusing on the fixed effect using the inverse variance method implemented in the software package METAL (Willer et al, 2010). In this approach, the effect size estimates (β-coefficients) are weighted according to their estimated standard errors. To determine statistically significant genetic associations, a marginal $P < 5.0 \times 10^{-8}$ in the meta-analysis was adopted as the threshold.

LD score regression and heritability estimation. To account for confounding factors such as population stratification and cryptic relatedness, we employed LD score regression intercepts (Bulik-Sullivan et al, 2015). This adjustment helped to ensure the accuracy of our analysis.

To estimate the heritability of the sweat gland phenotypes, we utilized LD score regression and genome-wide complex trait analysis incorporating the GREML algorithm (Yang et al, 2010). These methods allowed us to assess the genetic contribution to the phenotypes of interest.

Functional annotation. To generate regional plots, we utilized LocusZoom (http://locuszoom.sph.umich.edu/locuszoom/). To investigate the regulatory elements and functional annotations of SNPs, we employed multiple SNP annotation databases, including HaploReg, version 4.1 (Ward and Kellis, 2012); ENCODE (Encyclopedia of DNA elements) (ENCODE Project Consortium, 2004); REMC (Roadmap for Epigenomics Mapping) data (Kundaje et al, 2015); RegulomeDB (Boyle et al, 2012); and the UCSC genome browser (Zweig et al, 2008).

Transcription factor chromatin immunoprecipitation-sequencing peaks were annotated using CistromeDB (Qin et al, 2012). We retrieved lower loss-of-function observed/expected upper bound fraction scores from gnomAD (Karczewski et al, 2020).

To prioritize potentially causal SNPs for each locus, we employed a Bayesian approach with the PAINTOR software (Kichaev et al, 2014). This approach incorporated an LD matrix of pairwise correlation coefficients and functional annotation data. We constructed a 99% credible set consisting of SNPs that jointly attained or exceeded a 99% probability.

Tests for natural selection. To identify signals of positive selection, we utilized the Composite of Multiple Signals test (Grossman et al, 2010). The Composite of Multiple Signals test integrates signals from 5 different tests, namely, ΔiHH, iHS, XP-EHH, F_{ST}, and ΔDAF. We employed the genome-wide composite of multiple signals scores of individuals with

Northern and Western European ancestry in Utah (denoted as CEU), Yoruba in Ibadan (denoted as YRI), Japanese in Tokyo (denoted as JPT), and Han Chinese in Beijing (denoted as CHB) to assess potential signals of natural selection at loci related to sweating and sweat glands. The composite of multiple signals scores were obtained from the Broad Institute (https://pubs.broadinstitute.org/mpg/cmsviewer/).

To evaluate the evolutionary pressure on these loci, we calculated the ratios of nonsynonymous to synonymous nucleotide substitutions (Ka/Ks) using the kaks-calculator tool (Zhang et al, 2006) for each pair of orthologous genes.

Functional test using dual luciferase reporter assay. To construct *KCNAB2* enhancer reporters, we amplified fragments of 451 bp of *KCNAB2* by polymerase chain reaction from genomic DNA of 2 individuals homozygous with respect to the corresponding genotypes rs190550090 (TT and CC), using primers tailed with Nhe I and Xho I restriction sites for rs190550090, and directionally subcloned them into the pGL3-promter expression vector. We verified all recombinant clones by sequencing. A375 (human malignant melanoma) and human embryonic kidney 293 cells were cultured in high-glucose DMEM with 10% fetal bovine serum. For luciferase reporter assays, A375 and human embryonic kidney 293 cells were transfected with the indicated plasmids using the lipofectamine 2000 transfection reagent and incubated overnight at 37 °C or 31 °C (on the basis of the published protocol [Kim et al, 2003]) in 5% carbon dioxide condition. According to the manufacturer's instructions, luciferase activity was measured 36 hours after transfection using the Dual-Luciferase Reporter Assay System. All assays were performed in at least 3 replicates.

SUPPLEMENTARY REFERENCES

Asahina M, Poudel A, Hirano S. Sweating on the palm and sole: physiological and clinical relevance. Clin Auton Res 2015;25:153–9.

Boyle AP, Hong EL, Hariharan M, Cheng Y, Schaub MA, Kasowski M, et al. Annotation of functional variation in personal genomes using RegulomeDB. Genome Res 2012;22:1790–7.

Bulik-Sullivan BK, Loh PR, Finucane HK, Ripke S, Yang J, Schizophrenia Working Group of the Psychiatric Genomics Consortium, et al. LD Score regression distinguishes confounding from polygenicity in genome-wide association studies. Nat Genet 2015;47:291–5.

Chang CC, Chow CC, Tellier LC, Vattikuti S, Purcell SM, Lee JJ. Second-generation PLINK: rising to the challenge of larger and richer datasets. GigaScience 2015;4:7.

ENCODE Project Consortium. The ENCODE (ENCyclopedia of DNA elements) project. Science 2004;306:636–40.

Endo C, Johnson TA, Morino R, Nakazono K, Kamitsuji S, Akita M, et al. Genome-wide association study in Japanese females identifies fifteen novel skin-related trait associations. Sci Rep 2018;8:8974.

Grossman SR, Shlyakhter I, Karlsson EK, Byrne EH, Morales S, Frieden G, et al. A composite of multiple signals distinguishes causal variants in regions of positive selection [published correction appears in Science 2012;335:796. Shylakhter, Ilya [corrected to Shlyakhter, Ilya].]. Science 2010;327:883–6.

Howie BN, Donnelly P, Marchini J. A flexible and accurate genotype imputation method for the next generation of genome-wide association studies. PLoS Genet 2009;5:e1000529.

Juniper K Jr, Stewart Jr, Devaney GT, Smith TJ. Finger-tip sweat-gland activity and salivary secretion as indices of anticholinergic drug effect. Am J Dig Dis 1964;9:31–42.

Karczewski KJ, Francioli LC, Tiao G, Cummings BB, Alföldi J, Wang Q, et al. The mutational constraint spectrum quantified from variation in 141,456 humans. Nature 2020;581:434–43.

Kichaev G, Yang WY, Lindstrom S, Hormozdiari F, Eskin E, Price AL, et al. Integrating functional data to prioritize causal variants in statistical fine-mapping studies. PLoS Genet 2014;10:e1004722.

Kim DS, Park SH, Kwon SB, Joo YH, Youn SW, Sohn UD, et al. Temperature regulates melanin synthesis in melanocytes. Arch Pharm Res 2003;26:840–5.

Kundaje A, Meuleman W, Ernst J, Bilenky M, Yen A, et al. Integrative analysis of 111 reference human epigenomes. Nature 2015;518:317–30.

Landt SG, Marinov GK, Kundaje A, Kheradpour P, Pauli F, Batzoglou S, et al. ChIP-seq guidelines and practices of the ENCODE and modENCODE consortia. Genome Res 2012;22:1813–31.

Price AL, Patterson NJ, Plenge RM, Weinblatt ME, Shadick NA, Reich D. Principal components analysis corrects for stratification in genome-wide association studies. Nat Genet 2006;38:904–9.

Qin B, Zhou M, Ge Y, Taing L, Liu T, Wang Q, et al. CistromeMap: a KnowledgeBase and web server for ChIP-Seq and DNase-Seq studies in mouse and human. Bioinformatics 2012;28:1411–2.

Sato K, Dobson RL. Regional and individual variations in the function of the human eccrine sweat gland. J Invest Dermatol 1970;54:443–9.

Ward LD, Kellis M. HaploReg: a resource for exploring chromatin states, conservation, and regulatory motif alterations within sets of genetically linked variants. Nucleic Acids Res 2012;40:D930–4.

Willer CJ, Li Y, Abecasis GR. METAL: fast and efficient meta-analysis of genomewide association scans. Bioinformatics 2010;26:2190–1.

Yang J, Benyamin B, McEvoy BP, Gordon S, Henders AK, Nyholt DR, et al. Common SNPs explain a large proportion of the heritability for human height. Nat Genet 2010;42:565–9.

Zhang Z, Li J, Zhao XQ, Wang J, Wong GK, Yu J. KaKs_Calculator: calculating Ka and Ks through model selection and model averaging. Genomics Proteomics Bioinformatics 2006;4:259–63.

Zweig AS, Karolchik D, Kuhn RM, Haussler D, Kent WJ. UCSC genome browser tutorial. Genomics 2008;92:75–84.

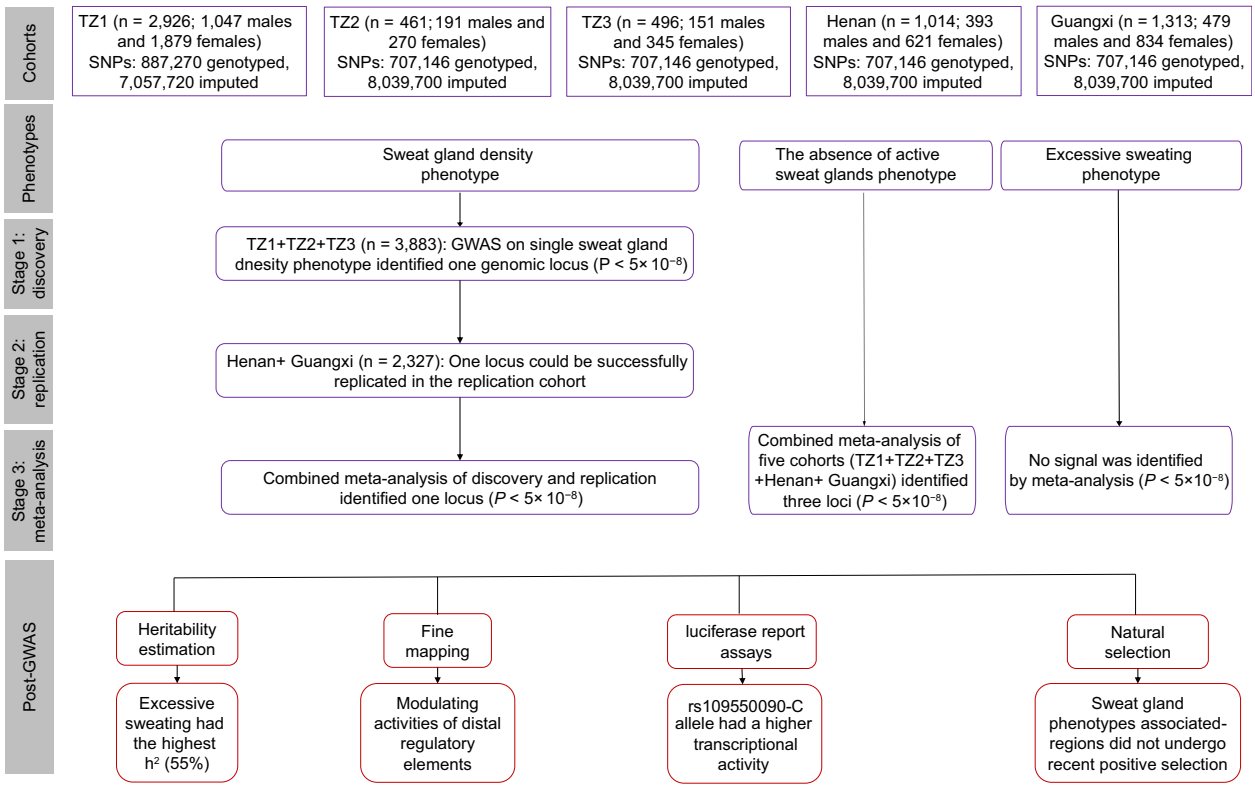

Supplementary Figure S1. Overview of the analysis.

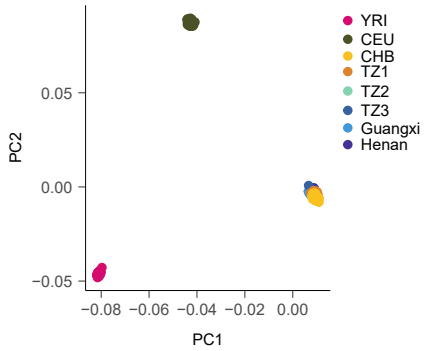

Supplementary Figure S2. The PCs analysis of 6210 samples and reference samples from the HapMap. PC, principal component.

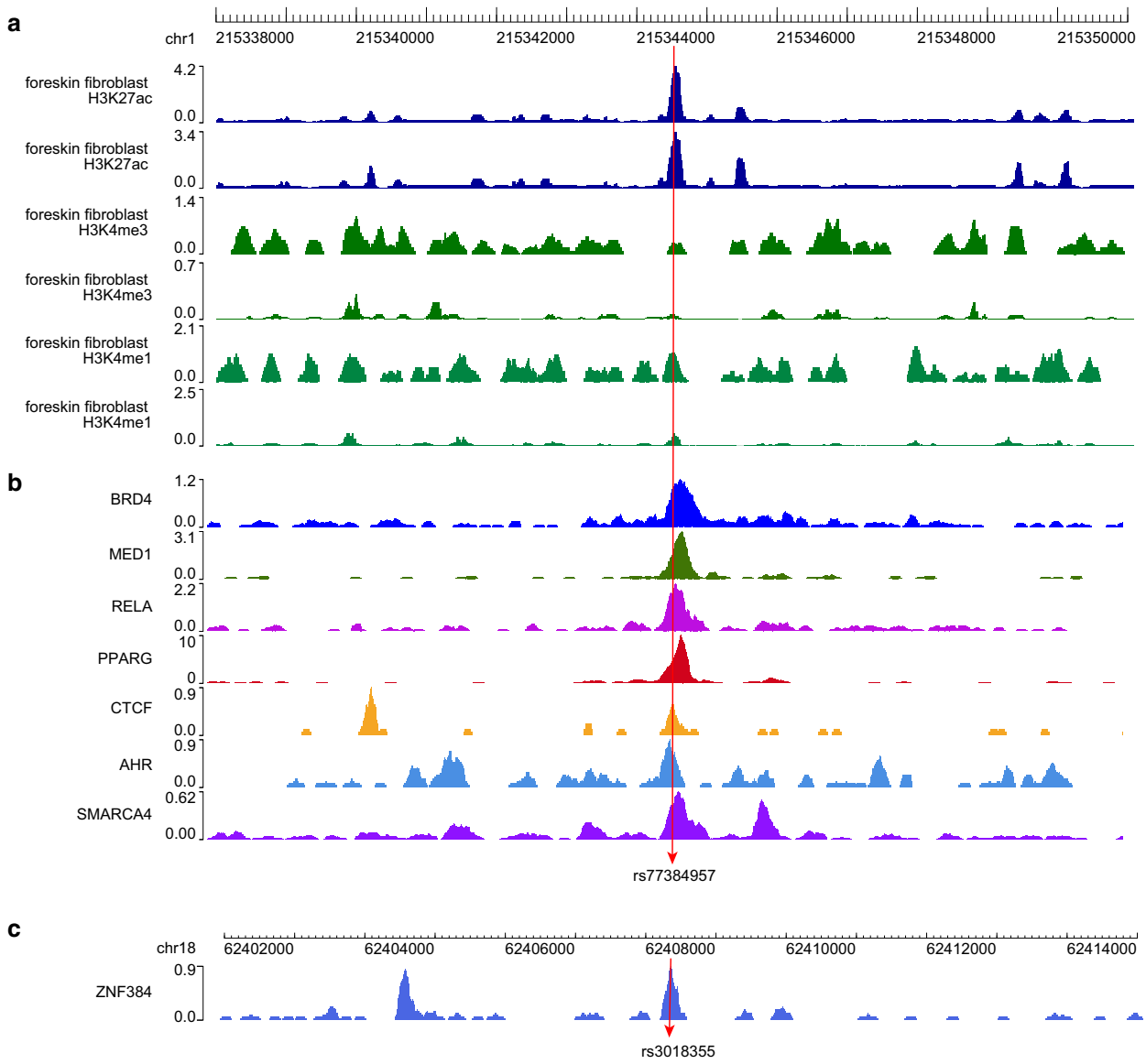

Supplementary Figure S3. Functional annotation of the absence of active sweat glands associated SNPs rs77384957 and rs3018355. (**a**) The absence of active sweat glands–associated SNP rs77384957 is bound by multiple histone modifications. (**b**) ChIP-Seq analysis reveals that the lead SNP rs77384957 serves as a binding site for transcription factors BRD4, MED1, RELA, PPARG, CTCF, AHR, and SMARCA4. (**c**) ChIP-Seq analysis demonstrates that the absence of active sweat glands phenotype–associated SNP rs3018355 serves as a binding site for the transcription factor ZNF384. ChIP-Seq, chromatin immunoprecipitation sequencing.

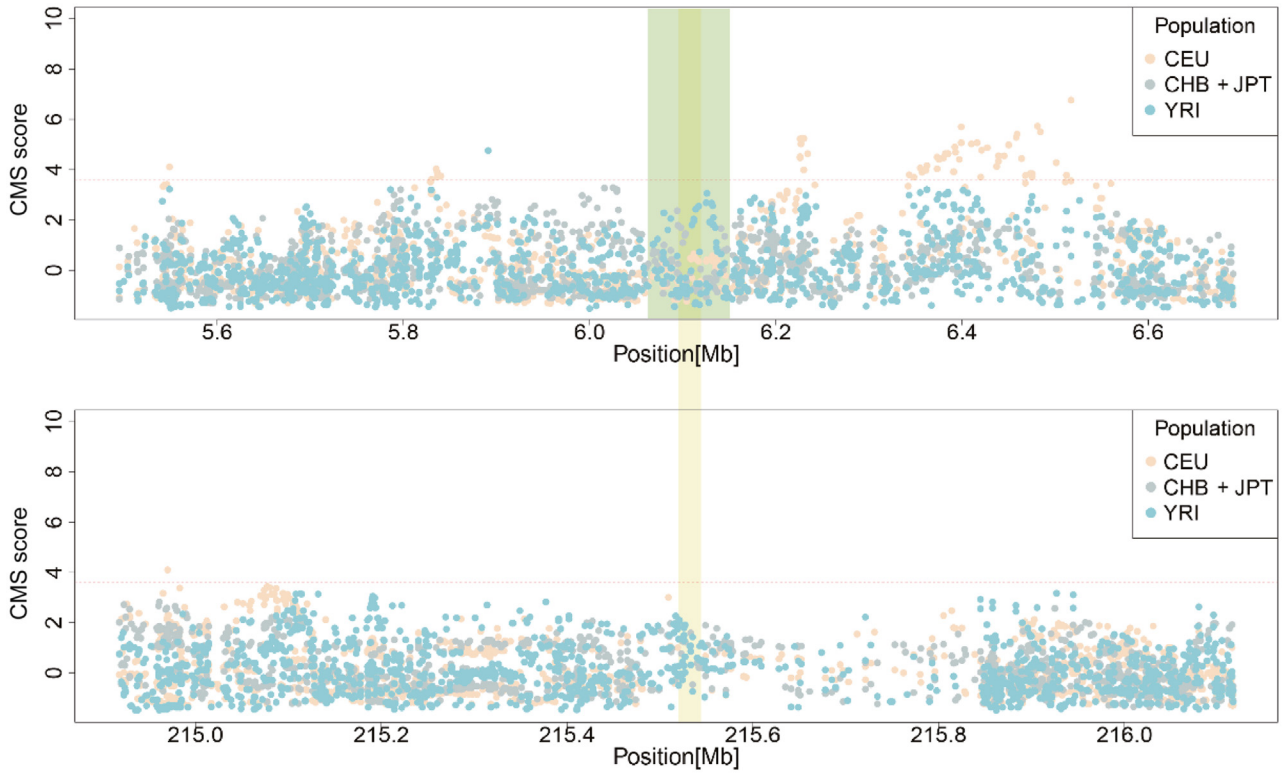

Supplementary Figure S4. CMS for the region extending 500 kb upstream and downstream of the Z-SGD–associated SNP rs190550090 (top) and the absence of active sweat glands–associated SNP rs77384957 (bottom). The yellow highlight indicates the loci associated with phenotypes, whereas the green color represents the *KCNAB2* genes. CMS, composite of multiple signal; Z-SGD, Z-transformed sweat gland density.

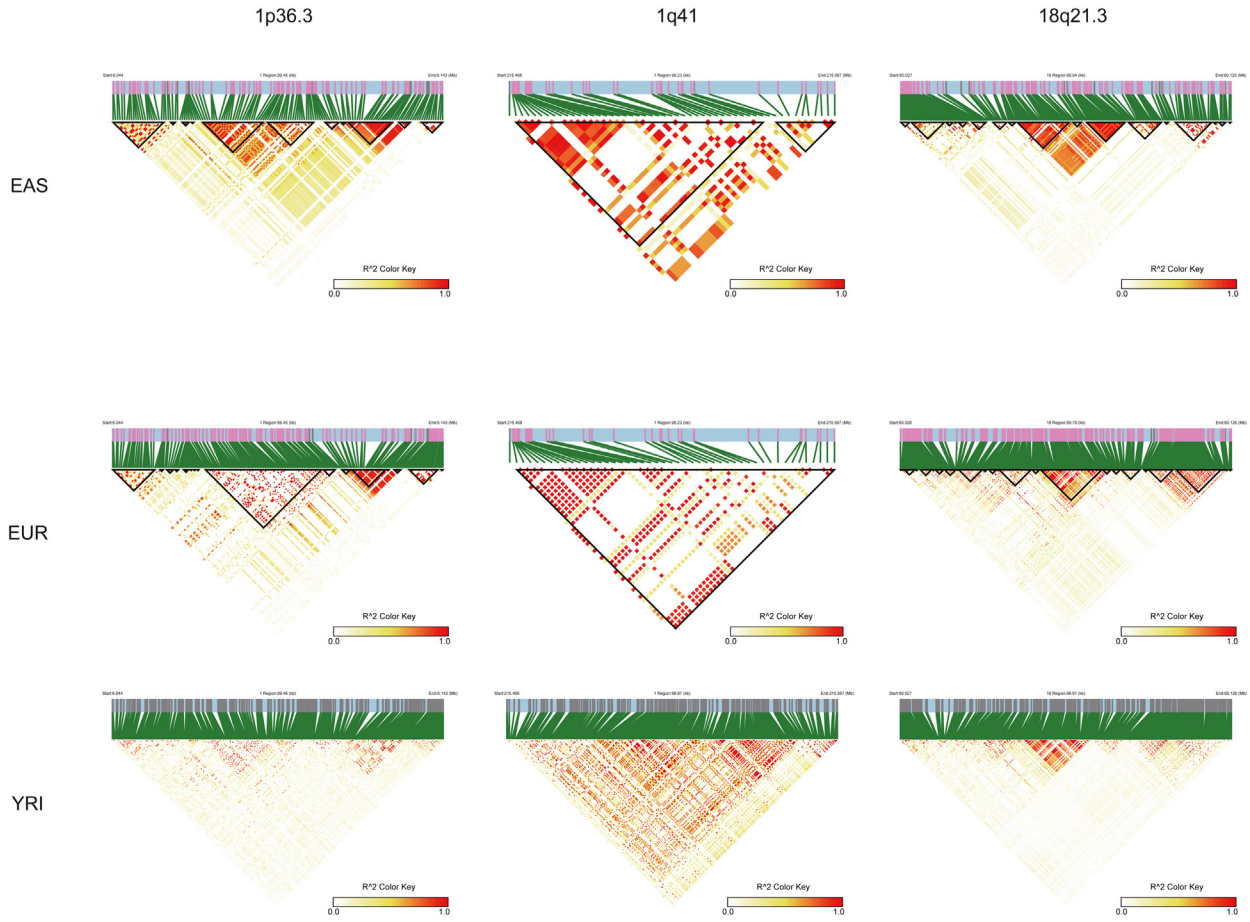

Supplementary Figure S5. The heatmap of pairwise LD (r^2) in the 3 identified marker SNPs (rs190550090 at 1p36.3, rs77384957 at 1q41, and rs3018355 at 18q21.3). LD, linkage disequilibrium.

Supplementary Figure S6. Image classification according to the quality.

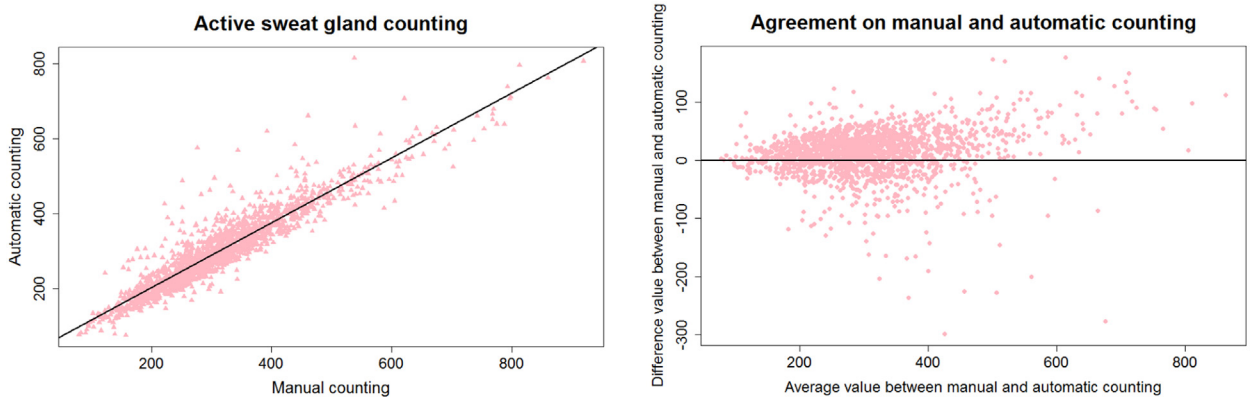

Supplementary Figure S7. A strong correlation and consistent agreement between the number of sweat glands recognized by our developed image recognition method and those manually labeled.

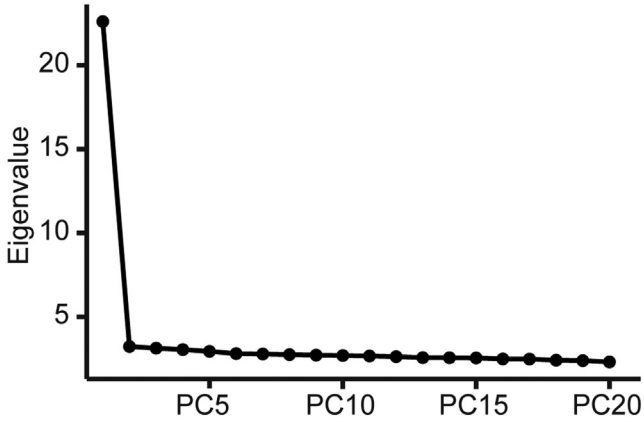

Supplementary Figure S8. Eigenvalues of genomic PCs. PC, principal component.